Journal of Materials Chemistry A

Accepted Manuscript

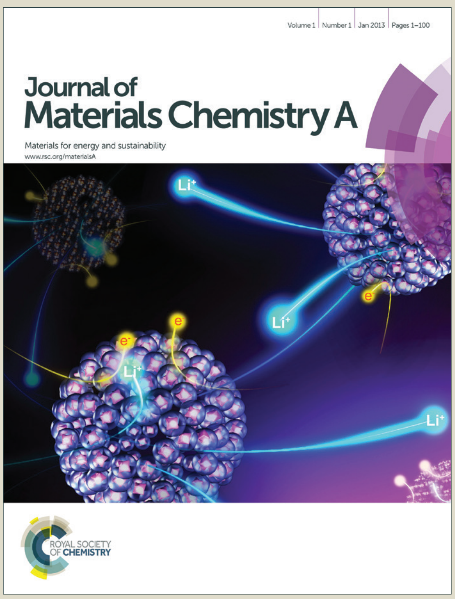

Graphic for Table of Contents

Design of Yolk-shell Fe_3O_4@PMAA Composite Microspheres for Adsorption of Metal Ions and pH-controlled Drug Delivery

Linling Zhao, Huarong Liu*, Fengwei Wang and Lai Zeng
Department of Polymer Science and Engineering, CAS Key Laboratory of Soft Matter Chemistry, University of Science and Technology of China, Hefei, Anhui 230026, China
*Corresponding author: Huarong Liu, E-mail: hrliu@ustc.edu.cn

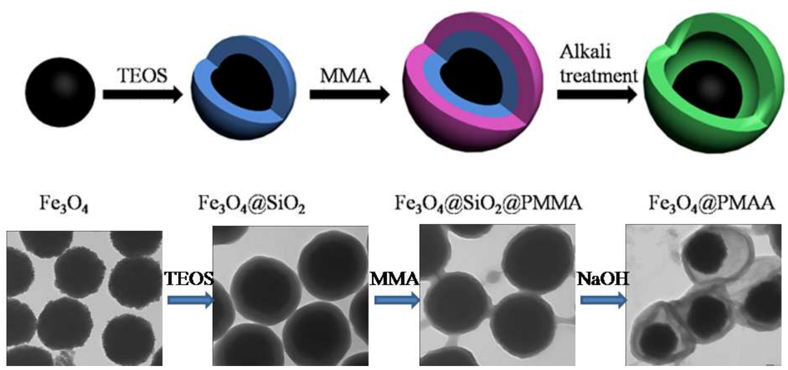

Yolk-shell structured pH-responsive Fe_3O_4@PMAA microspheres have been prepared for adsorption of metal ions and drug delivery via combined sol-gel reaction, emulsion polymerization and selective etching methods accompanying with hydrolysis of PMMA shell in core-shell-shell Fe_3O_4@SiO_2@PMMA composite microspheres.

Cite this: DOI: 10.1039/c0xx00000x

www.rsc.org/xxxxxx

ARTICLE TYPE

Design of Yolk-Shell Fe_3O_4@PMAA Composite Microspheres for Adsorption of Metal Ions and pH-controlled Drug Delivery

Linling Zhao, Huarong Liu*, Fengwei Wang and Lai Zeng

Received (in XXX, XXX) Xth XXXXXXXXX 20XX, Accepted Xth XXXXXXXXX 20XX

DOI: 10.1039/b000000x

Core-shell-shell structured Fe_3O_4@SiO_2@PMMA composite microspheres were synthesized in large scale via combined sol-gel reaction and seeded emulsion polymerization. The yolk-shell structured Fe_3O_4@PMAA microspheres with pH-responsive shell were then produced after the etching of silica interlayer and meanwhile the hydrolysis reaction of the PMMA shells in NaOH aqueous solution. The resulting microspheres with tunable void space and shell thickness were characterized by transmission electron microscopy (TEM), Fourier transform infrared spectroscopy (FTIR), and dynamic laser scattering (DLS). The effect of shell thickness and void space of yolk-shell Fe_3O_4@PMAA microspheres on the adsorption of metal ions and drug delivery was investigated. The results demonstrated the excellent adsorption capacity of Cu^{2+} and Pb^{2+} and reusable ability for Cu^{2+} using the optimum Fe_3O_4@PMAA microspheres as adsorbent in a weak acidic condition, as well as the high loading capacity and pH-controlled releasing ability of yolk-shell Fe_3O_4@PMAA microspheres by loading ceftriaxone sodium and controlled release study.

Introduction

During the past decades, yolk-shell microspheres (YSMs) with movable cores and enclosed large cavities have attracted a great deal of attention because of their potential applications in drug delivery,[1] biomedical,[2] catalysis,[3] lithium-ion batteries[4, 5] and so on owing to their unique properties, such as low density, excellent loading capacity and multi-functionality.[6] Various YSMs with controllable size and shape, such as Au@SiO_2,[7] SiO_2@TiO_2@polyaniline,[8] Au@Ag[9] and SiO_2@SiO_2,[10] have been fabricated by different methods, including template-assisted selective etching, Kirkendall or Ostwald ripening, bottom-up or soft templating, and ship-in-bottle processes.[11] Although some progress in the synthesis of YSMs has been achieved, most of the above methods are only work on microspheres with particular compositions and structures.[12] Moreover, the reported YSMs are mainly inorganic materials.[6] Recently, some efforts have been devoted to the synthesis of inorganic/organic hybrid YSMs[13-15] due to their synergistic and hybrid properties derived from several components. Among them, yolk-shell microspheres with magnetic core and functional stimuli-responsive polymer shell[16] is especially compelling because magnetic core may provide targeted delivery, magnetic resonance imaging, separability and recyclability,[17] while stimuli-responsive polymer shell can not only prevent magnetic particles from aggregating, improve their chemical stability, and decrease their potential toxicity, but also change polymer chain conformation in direct response to stimuli, e.g. pH, ionic strength and temperature, making these YSMs suitable for applications in drug and gene delivery,[18] biomedical,[19] catalysis,[20] and biosensors.[21] For example, Zhang *et al.*[22] fabricated the multifunctional fluorescent-magnetic polyethyleneimine functionalized Fe_3O_4/mesoporous silica yolk-shell microcapsules by selective dissolution method for magnetically guided small interfering RNA delivery. Yao and his co-workers[23] prepared yolk-shell Fe_3O_4@Polypyrrole microspheres with high magnetization via selective etching method for their applications as catalyst supports. Therefore, until now the template-assisted selective etching method is the simple and useful way to produce YSMs with inorganic core and functional polymer shell in which the core particles is coated with double shells consisting of different materials, the inner shell is then selectively removed by using a suitable solvent. This method can obtain YSMs with various compositions and non-spherical structure, as well control their void space and shell thickness. However, the relevant work about stimuli-responsive YSMs with magnetic core has rarely been reported yet.

Poly(methacrylic acid) (PMAA), a hydrophilic stimuli-responsive polymer, is attractive for a wide number of applications because it can respond to pH changes through reversible structural transitions and self-adjustment of physicochemical properties.[24] At present, PMAA is often coated on the inorganic cores by RAFT polymerization[25] and distillation-precipitation polymerization.[26] However, RAFT polymerization method often results in quite thin thickness of the PMAA shell and difficult post-treatment of the product due to the peculiar RAFT reagent. Up to now, the distillation-precipitation polymerization is a barely powerful technique for coating hydrophilic polymer on the inorganic particles. Nonetheless, its production rate is considerable lower than desirable and the solvent acetonitrile is high toxicity, resulting in the diseconomy of the distillation-precipitation polymerization. Therefore, it remains a great challenge to develop a general and effective synthetic method for preparing inorganic/hydrophilic polymer hybrid YSMs.

In this report, we present a facile route for the preparation of pH-responsive yolk-shell Fe_3O_4@PMAA microspheres via combined sol-gel reaction, emulsion polymerization and selective etching methods (Scheme 1). Emulsion polymerization is the most simple and efficient method to synthesis organic/inorganic composite latexes.[27] However, for hydrophilic monomers, such as MAA, it is not facile to coat on the Fe_3O_4@SiO_2 particles with PMAA shells by direct polymerization because the polymerization of MAA occurs in the continuous phase of emulsion which easily implode to form PMAA gel.[28] So we first prepare core-shell-shell Fe_3O_4@SiO_2@PMMA composite microspheres via seeded emulsion polymerization, then during selective etching of silica interlayer in alkaline solution, the PMMA shell will hydrolyze into pH-responsive PMAA shell.[29] The void space of yolk-shell Fe_3O_4@PMAA microspheres and the thickness of the PMAA shell can be controlled by changing the amounts of precursor and monomer, respectively. The as-prepared yolk-shell Fe_3O_4@PMAA microspheres are ideal candidates for the micro-sized adsorbents of heavy metal ions owing to the following reasons: (1) The abundant carboxyl groups in the PMAA shell can form strong complexes with metal ions;[30] (2) The hydrophilic thin shell may serve as permeable membrane for metal ion transport;[31] (3) The presence of void space in the yolk-shell structure can enhance the adsorption capacities of metal ions.[32] (4) Different from conventional methods such as chemical precipitation, electrodialysis and ultrafiltration, magnetic separation is easy and highly efficient with low cost. To the best of our knowledge, the work on the yolk-shell microspheres as adsorbents of heavy metal ions has not been reported. Considering the practical applications, the regeneration and reuse of the magnetic yolk-shell Fe_3O_4@PMAA microspheres as adsorbent was investigated. The as-prepared yolk-shell Fe_3O_4@PMAA microspheres are also a powerful platform for drug delivery and controlled release. Ceftriaxone sodium (CTX), a water soluble anti-inflammatory drug, is chosen as a model drug to demonstrate the high loading capacity and controlled release of the yolk-shell Fe_3O_4@PMAA composite microspheres.

Experimental section

Materials

Iron (III) chloride hexahydrate ($FeCl_3\cdot6H_2O$), tetraethyl orthosilicate (TEOS), sodium acetate (NaOAc), trisodium citrate (Na_3Cit), aqueous ammonia solution ($NH_3\cdot H_2O$, 28%), potassium persulfate (KPS), potassium dihydrogen phosphate (KH_2PO_4), sodium hydroxide (NaOH), concentrated hydrochloric acid (37%, HCl), nitric acid (HNO_3), sodium chloride (NaCl), ethylene glycol (EG), diethylene glycol (DEG), methyl methacrylate (MMA), copper chloride ($CuCl_2$), lead nitrate ($Pb(NO_3)_2$), chromium nitrate ($Cr(NO_3)_3$), cadmium chloride ($CdCl_2$) and anhydrous ethanol were purchased from Sinopharm Chemical Reagent Co., Ltd., in which MMA was distilled under reduced pressure and KPS was recrystallized from distilled water before use, while the rest were used as received. Divinyl benzene (DVB) and 3-methacryloxypropyltrimethoxy-silane (MPS) were purchased from Sigma-Aldrich and used without any further treatment. Ceftriaxone sodium (CTX) was purchased from Shanghai Roche Pharmaceuticals Ltd. and used as received. Deionized water was used in the experiments.

Synthesis of Monodisperse Fe_3O_4 particles

In this work, a modified solvothermal method[33] was developed to construct superparamagnetic Fe_3O_4 particles. 1.08 g of $FeCl_3\cdot6H_2O$, 0.25 g of trisodium citrate and 1.6 g of sodium acetate were dissolved in a mixture of EG (40 ml) and DEG (10 ml) under vigorous stirring for 30 min. The obtained homogeneous yellow solution was then transferred into a Teflon-lined stainless-steel autoclave for heating 10 h at 200°C. After that, the autoclave was carefully taken out to cool down to room temperature. The obtained Fe_3O_4 particles were thoroughly washed with ethanol and deionized water for several times, and finally vacuum dried at 25°C for 12 h for further use.

Synthesis and Surface Modification of Magnetic Fe_3O_4@SiO_2 Composite Microspheres

To synthesize Fe_3O_4@SiO_2 microspheres, the SiO_2 shell was prepared through a modified Stöber method.[34] In a typical process, 25 mg of Fe_3O_4 particles were fully dispersed in a solution containing ethanol (20 ml), H_2O (1 ml) and concentrated ammonia (28 wt%, 0.5 ml) under ultrasonic vibration. Then, 0.05 ml of TEOS was injected into the solution every 20 min until the total amount of TEOS reached 0.25 ml, followed by mechanically stirring for 6 h at 30°C. The obtained Fe_3O_4@SiO_2 microspheres were washed with ethanol and deionized water for several times to remove blank silica nanoparticles. The other two Fe_3O_4@SiO_2 microspheres samples with different thickness of SiO_2 were made in similar way just by increasing the volume of TEOS to 0.5 ml and 0.8 ml, respectively. In order to modify the surface of Fe_3O_4@SiO_2 microspheres with vinyl group, the purified Fe_3O_4@SiO_2 microspheres (40 mg) were re-dispersed in 40 ml of ethanol, and then 0.5 ml of MPS was added to the dispersion. After mechanically stirred for 48 h at 30°C, the modified Fe_3O_4@SiO_2 microspheres were washed with ethanol with the help of a magnet, and re-dispersed in 20 ml of ethanol for further use.

Synthesis of Core-shell-shell Fe_3O_4@SiO_2@PMMA Composite Microspheres

The Fe_3O_4@SiO_2@PMMA microspheres were synthesized via seeded emulsion polymerization. Typically, 5 ml of ethanol dispersion of Fe_3O_4@SiO_2-MPS microspheres were mixed with 30 ml of aqueous solution containing 0.003 g of SDS by mechanical stirring. After being degassed with nitrogen for 30 min, the monomer MMA (0.5 g) and crosslinker DVB (0.05 g) were added, and the solution was heated up to 70°C, then 0.5 ml of KPS aqueous solution (0.2 mg ml^{-1}) was added into the above dispersion to initiate the polymerization. After 7 h of reaction, the final products were collected by magnetic separation, washed with ethanol and deionized water several times, and finally re-dispersed in deionized water. We also prepared other samples just via changing the amount of MMA monomer (0.3 g and 1.2 g) to demonstrate that the thickness of PMMA shell can be tuned.

Synthesis of pH-responsive Fe_3O_4@PMAA Yolk-Shell Microspheres

Yolk-shell structured Fe_3O_4@PMAA microspheres were prepared by the removal of silica interlayer and the hydrolysis reaction of PMMA in 8 mol L^{-1} NaOH aqueous solution for 24 h. The obtained Fe_3O_4@PMAA microspheres were washed with ethanol and water three times, respectively, and finally vacuum dried at 40°C for 12 h for further use.

Yolk-Shell Fe_3O_4@PMAA Microspheres as Adsorbent for Adsorption of Metal Ions and Reused Cycles

Adsorption of different metal ions by yolk-shell Fe_3O_4@PMAA microspheres were performed in batch mode. Herein, we have used the following metal ions Cd^{2+}, Pb^{2+}, Cu^{2+} and Cr^{3+} for the adsorption tests. In a typical experimental setup, metal salts ($CdCl_2$, $Pb(NO_3)_2$, $CuCl_2$ and $Cr(NO_3)_3$) as metal ions precursor were dissolved in deionized water to prepare 10 mmol L^{-1} metal ion solutions in which a small amount of hydrochloric acid solution were added to adjust the pH value of solutions. Absorbent Fe_3O_4@PMAA microspheres (10 mg) were added to 100 ml of metal ion solutions with different pH value (pH=2, 3, 4, 5, 6 and 7) and then the resulting dispersion was shaken in Thermostatic Water Bath Oscillator (WHY-2) at 25°C for 6 h. After then, the absorbents were removed immediately by magnetic separation with the help of a magnet and the supernatant liquids were analysed by plasma atomic emission spectrometer to measure the concentration of metal ions. The amount of metal ions adsorbed on Fe_3O_4@PMAA at adsorption equilibrium, q_e (mmol g^{-1}), was calculated by the following equations:

$$q_e = \frac{(C_0 - C_e) \times V}{W \times A} \qquad (1)$$

Where C_0 and C_e are the initial and equilibrium concentration of metal ions (mg L^{-1}), respectively, V is the volume of metal ion solution (L), A is the relative atomic weight of metal ions (mg $mmol^{-1}$) and W is the weight of absorbents (g). The affect of thickness of PMAA shells and void space of the Fe_3O_4@PMAA microspheres on adsorption capacities were carried out by various Fe_3O_4@PMAA samples (see Table S1) using Pb^{2+} as adsorbate metal ion at pH 6 value.

The content of carboxylic groups on the shell of Fe_3O_4@PMAA microspheres was indirectly determined by the measurement of electric conductivity. First, 0.1 g of the Fe_3O_4@PMAA microspheres was dispersed in 200 ml of deionized water, and then 20 ml of 0.01 mol L^{-1} HCl solution was added under stirring. Finally, 0.01 mol L^{-1} NaOH solution (calibrated by potassium hydrogen phthalate) was added dropwise into the above dispersion, and the change of the electric conductivity was recorded to evaluate the content of carboxylic groups.

In a typical desorption test of metal ions from the Fe_3O_4@PMAA microspheres, the above Cu^{2+}-adsorbed Fe_3O_4@PMAA adsorbents was added into 50 ml of 1 mol L^{-1} HNO_3 aqueous solution, and the obtained suspension was then shaken in Thermostatic Water Bath Oscillator at 25°C for 30 min,[35] followed by ultrasonication for 30 min. Finally, the adsorbents were collected by a magnet and reused for adsorption of Cu^{2+} at pH=5 again. The supernatant liquids of desorption and re-adsorption were analysed by plasma atomic emission spectroscopy to measure the concentration of metal ions. The cycles of desorption-adsorption processes were successively conducted at most 8 times.

Preparation of CTX-loaded Fe_3O_4@PMAA Microspheres and the Drug Release Studies

CTX was loaded into yolk-shell Fe_3O_4@PMAA composite microspheres by the following method. Typically, 10 mg of Fe_3O_4@PMAA microspheres were added to 20 ml of 1 mg ml^{-1} CTX solution and the mixture was kept in a shaker (SK-O180-Pro) for 48 h. Finally, the CTX-loaded Fe_3O_4@PMAA microspheres were collected by magnetic separation and washed three times with deionied water to remove the unbound drug molecules. The absorbance of the supernatant fluid at 272 nm was monitored by UV-Vis spectrophotometer. The amount of CTX loaded into the microspheres was determined from a calibration curve obtained from the absorbance for a series of CTX solutions at different concentrations (as shown in Fig. S3). The drug loading capacity (DLC) was determined by the following equations:

$$DLC(\%) = \frac{W_L}{W_m} \times 100 \qquad (2)$$

Where DLC is drug loading capacity; W_L is the weight of drug (mg) in microspheres; W_m is the original weight (mg) of microspheres.

The cumulative drug release experiments were carried out at different pH values to evaluate the pH-responsive behaviour of the Fe_3O_4@PMAA microspheres. The release amount of CTX from the CTX-loaded Fe_3O_4@PMAA microspheres was checked in a different phosphate buffer solution (PBS) at pH=4.5 and pH=7.5, respectively, by spectrophotometric method (at 272 nm) at regular time intervals. The percentage of released drug was calculated from a standard curve of free drug solution (Fig. S3). The ionic strength of all PBS was tuned to equal value of 0.2 mol L^{-1} using NaCl aqueous solution. Also, the affect of thickness of PMAA shells and void space of Fe_3O_4@PMAA microspheres on drug loading capacity and drug release were carried out by various Fe_3O_4@PMAA samples.

Characterization Methods

The structure and morphology of samples were characterized by transmission electron microscope (TEM; Hitachi Model H-7560). All samples were dried onto Formvar-coated copper grids before examination. Powder X-ray diffraction (XRD) patterns were recorded on a Rigaku D/max γ_A diffractometer equipped with graphite monochromatized Cu Kα irradiation (λ=0.154178 nm) at 30 kV and 150 mA. The crystal size of magnetic particles was estimated by applying the Scherrer's formula, namely $D = k\lambda/(\beta\cos\theta)$, where D is the crystallite size, λ is the X-ray wavelength, k is a geometric factor which has a typical value of about 0.9, θ is the Bragg angle, and β (in radians) is the full width at half maximum (FWHM) of the diffraction peak at 2θ. Fourier transform infrared (FTIR) spectra were determined on a VECTOR-22 FTIR spectrometer over potassium bromide pellet. The magnetic properties of the samples were investigated at

300K using a vibrating sample magnetometer (VSM). Hydrodynamic diameters (Dh) and zeta potentials of the microspheres at a different pH value were measured by dynamic light scattering (DLS) at room temperature using a commercial spectrometer (ALV/DLS/SLS-5022F) equipped with a multitau digital time correlator (ALV5000) and a cylindrical 22mV UNIPHASE He-Ne laser (λ_0 =632 nm) as the light source. The content of carboxylic groups in Fe_3O_4@PMAA microspheres was determined by conductivity meter (DDS-L700). Plasma atomic emission spectrometer (ICP-AES, Optima 7300DV) was employed to measure the concentration of metal ions in the solution for the adsorption or desorption of metal ions. The drug loading and release processes was monitored by absorption spectrophotometer (Shimadzu UV-1700).

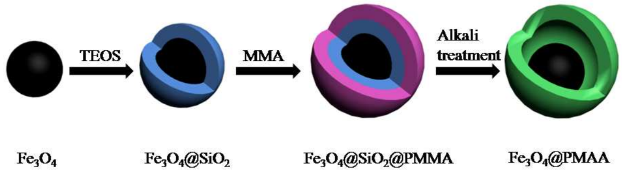

Scheme 1 Schematic Illustration of the Approach for the Preparation of Yolk-Shell Fe_3O_4@PMAA Composite Microspheres

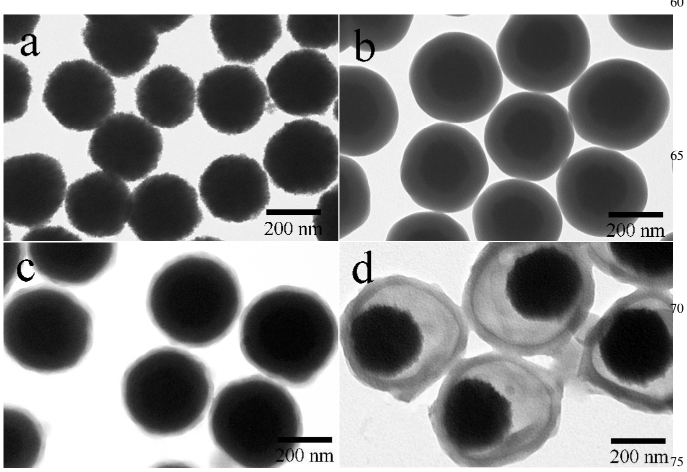

Fig. 1 TEM images of the as-prepared samples: a) Fe_3O_4 particles; b) Fe_3O_4@SiO_2 microspheres; c) Fe_3O_4@SiO_2@PMMA microspheres; d) Fe_3O_4@PMAA microspheres.

Results and discussion

The protocol for the synthesis of pH-responsive yolk-shell Fe_3O_4@PMAA composite microspheres is illustrated in Scheme 1. First, monodisperse and uniform Fe_3O_4 particles (Fig. 1a) prepared by a one-step modified solvothermal method[33] are coated with silica layer via a versatile sol-gel process using TEOS as a precursor. Second, the Fe_3O_4@SiO_2 particles (Fig. 1b) are encapsulated in polymer via a seeded emulsion polymerization to obtain monodisperse Fe_3O_4@SiO_2@PMMA composite microspheres (Fig. 1c). Finally, the interlayer silica of the composite microspheres is selectively dissolved by 8 mol L^{-1} NaOH aqueous solution, while the PMAA shell is simultaneously formed from the hydrolysis reaction of PMMA in alkaline solution,[29] and thus the pH-responsive yolk-shell Fe_3O_4@PMAA microspheres are obtained as shown in Fig. 1d.

Fe_3O_4@SiO_2@PMMA Core-shell-shell Composite Microspheres

Water-dispersible uniform Fe_3O_4 particles were first produced by a modified solvothermal reaction at 200°C with acetate sodium as alkaline resources, trisodium citrate as electrostatic stabilizer and EG/DEG as both solvent and reducing agent. Fig. 1a shows the representative TEM image of the as-prepared monodisperse Fe_3O_4 spherical particles with an average size of about 200±11 nm. It is noteworthy that each Fe_3O_4 particle was composed of many primary nanocrystals, which is consistent with previous literature.[36] The formation mechanism of Fe_3O_4 particles follows the well-documented two-stage growth model in which primary nanocrystals nucleate first in a supersaturated solution and then aggregate into large secondary particles[37] with the spherical morphology due to minimizing the interfacial free energy between the particles and the medium.[38] FT-IR spectrum of Fe_3O_4 particles in Fig. 2a shows the two characteristic absorption peaks at 582 cm^{-1} and 1635 cm^{-1}. The former is attributed to the Fe-O stretching vibration and the latter is assigned to the carboxylate on the surface of the Fe_3O_4 particles because of the carboxyl groups anchoring on the particle surface during the solvothermal reaction.[25] Therefore, these Fe_3O_4 particles are stable in solution.

The Fe_3O_4@SiO_2 composite microspheres were obtained by a sol-gel process via the controlled hydrolysis of various TEOS amount in the presence of Fe_3O_4 particles as seeds. As shown in Fig. 1b, the Fe_3O_4@SiO_2 composite microspheres with an average diameter of 250 nm exhibit a relatively smooth surface and a uniform well-defined core-shell structure due to the deposition of the silica layer. Moreover, the different thickness of silica interlayer can be realized, which will be described in detail later. Fig. 2b shows the FTIR spectrum of Fe3O4@SiO_2 composite microspheres, which further confirms the encapsulation of Fe_3O_4 particles in silica shells. A strong absorption peak at 1095 cm^{-1} is attributed to the Si-O-Si of silica shell, and that at 3400 cm^{-1} is assigned to the –OH groups on the surface of the silica. At the same time, the weakening of the Fe-O absorption peak at 583 cm^{-1} is also owing to the silica shell coated on the surface of Fe_3O_4 particles.

Before the synthesis of Fe_3O_4@SiO_2@PMMA composite microspheres, Fe_3O_4@SiO_2 microspheres were modified with MPS through the hydrolytic condensation between the hydroxyl groups on the surface of silica and methoxyl groups of MPS. Then, the active vinyl double bond of MPS would allow the copolymerization of monomers MMA and DVB on the surface of the Fe_3O_4@SiO_2 microspheres to form crosslinked PMMA outer shell. As shown in Fig. 1c, the Fe_3O_4@SiO_2@PMMA composite microspheres with a mean diameter of 270 nm are slightly larger than Fe_3O_4@SiO_2 microspheres. Two new absorption peaks appearing at 1730 and 2950 cm^{-1} in the FTIR spectrum (Fig. 3c) are attributed to the stretching vibration of the ester C=O and C-H groups of the repeating MMA units, respectively, which further verifies the formation of PMMA shell.

The crystal structure of the as-prepared samples was examined by XRD. Fig. 3a shows a typical XRD pattern of the obtained Fe_3O_4 particles, where five strong characteristic diffraction peaks of (112), (211), (220), (303) and (224) can be indexed as the body-centered cubic magnetite (Fe_3O_4) crystallite by comparison

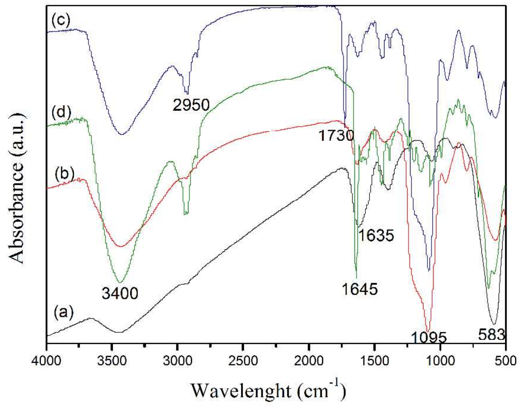

Fig. 2 FTIR absorbance spectra of (a) Fe_3O_4 particles; (b) Fe_3O_4@SiO_2 microspheres; (c) Fe_3O_4@SiO_2@PMMA composite microspheres; (d) Yolk-shell structured Fe_3O_4@PMAA microspheres.

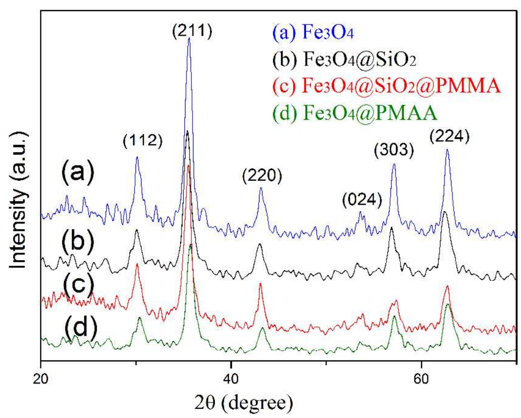

Fig. 3 XRD patterns of (a) Fe_3O_4 particles; (b) Fe_3O_4@SiO_2 microspheres; (c) Fe_3O_4@SiO_2@PMMA composite microspheres; (d) Fe_3O_4@PMAA microspheres.

with the standard JCPDS card file No. 75-1609. No obvious XRD peak arising from impurities was detected in the pattern, indicating that Fe_3O_4 particles were successfully prepared in high purity. Moreover, the broadening diffraction peaks indicate that these Fe_3O_4 particles have a small crystal size of 11.5 nm calculated from Scherrer's formula, which is consistent with the TEM result in Fig. 1a. Fig. 3(b, c, d) show the typical XRD patterns of Fe_3O_4@SiO_2 microspheres and core-shell-shell Fe_3O_4@SiO_2@PMMA microspheres as well as yolk-shell Fe_3O_4@PMAA microspheres, which are almost the same as that of Fe_3O_4 particles. No characteristic peak corresponding to silica is observed, suggesting the formation of amorphous silica. These results indicate that the coating of silica and polymer did not alter the crystalline structure of Fe_3O_4 particles.

The pH-responsive Yolk-shell Fe_3O_4@PMAA Composite Microspheres with Controllable Void Space and Shell Thickness

Yolk-shell structured pH-responsive Fe_3O_4@PMAA composite microspheres with different shell thickness and tunable void spaces have been fabricated by a rapid and simple template method. Because PMAA can be readily obtained from the hydrolysis of PMMA in an alkaline aqueous solution,[39] we etch the silica interlayer using 8 mol L^{-1} NaOH aqueous solution to obtain the yolk-shell Fe_3O_4@PMAA composite microspheres. The TEM image of yolk-shell Fe_3O_4@PMAA composite microspheres (Fig. 1d) reveals that the silica shells have been successfully removed from the core-shell-shell Fe_3O_4@SiO_2@PMMA composite microspheres. The FTIR spectrum of Fe_3O_4@PMAA microspheres is shown in Fig. 2d. The disappearance of Si-O-Si absorption peak at 1095 cm^{-1} also indicates that the SiO_2 layer of Fe_3O_4@SiO_2@PMMA composite microspheres of is etched completely. At the same time, the new characteristic absorption peak at 1645 cm^{-1} attributed to the –COOH groups of the repeating MAA units together with the disappearance of the absorption peak of ester C=O at 1730 cm^{-1} suggest the successful hydrolysis of PMMA. Moreover, the enhancement of the Fe-O absorption peak at 583 cm^{-1} is owing to the etching of SiO_2 layer. In addition, Fig. S1 shows the characteristic absorption peak of protonated carboxylic acid at 1460 cm^{-1} in a phosphate buffer solution at pH=4.5 (Fig. S1a), while that of deprotonated carboxylic acid at 1640 cm^{-1} at pH=10 (Fig. S1b). These results demonstrate that PMAA shells have been generated by the hydrolysis reaction of PMMA and they can respond to pH changes.

The thickness of interlayer silica can definitely influence the void volume of Fe_3O_4@PMAA yolk-shell microspheres. Therefore, good control over the thickness of silica interlayer is very important. The thickness of silica interlayer can be precisely tailored by changing the TEOS amount while keeping the amount of Fe_3O_4 seeds and solvent constant. As shown in Fig. 4(a-c), when the TEOS amount increases from 0.25 to 0.5 and 0.8 ml, the thickness of the silica shell for the Fe_3O_4@SiO_2 composite microspheres is varied from ~41 to ~74 and ~116 nm, respectively. Accordingly, the void space of the corresponding Fe_3O_4@PMAA microspheres increases obviously as shown in Fig. 4(d-f).

The thickness of the pH-responsive PMAA shell of yolk-shell structured Fe_3O_4@PMAA composite microspheres can also be

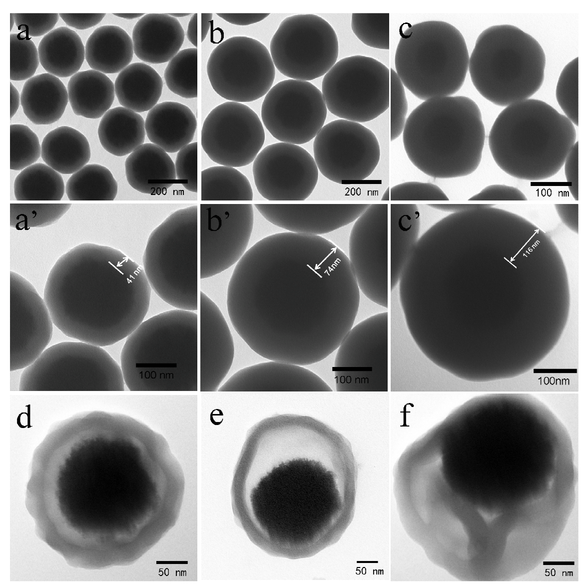

Fig. 4 TEM images of Fe_3O_4@SiO_2 composite microspheres at TEOS/Fe_3O_4 weight ratio of (a, a') 10:1; (b, b') 20:1; (c, c') 30:1. (a'-c') are high magnification images of (a-c), respectively. TEM images of the yolk-shell Fe_3O_4@PMAA composite microspheres using aforementioned corresponding Fe_3O_4@SiO_2 microspheres with different silica thickness as template: d) 41 nm, e) 76 nm and f) 116 nm.

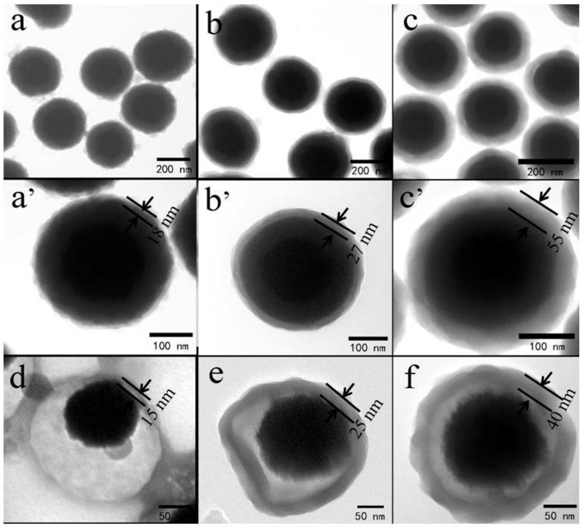

Fig. 5 TEM images of the Fe_3O_4@SiO_2@PMMA core-shell microspheres with different PMMA shell thickness: (a, a') 18 nm; (b, b') 27 nm; (c, c') 55 nm. (a'-c') are high magnification images of (a-c), respectively. TEM images of the Fe_3O_4@PMAA microspheres with different shell thickness prepared from the aforementioned corresponding Fe_3O_4@SiO_2@PMMA microspheres: (d) 15 nm; (e) 25 nm; (f) 40 nm.

tuned to meet different application requirements via controlling the thickness of the outer shell PMMA of Fe_3O_4@SiO_2@PMMA composite microspheres by changing the feeding amount of monomer MMA in the case of keeping the weight of Fe_3O_4@SiO_2-MPS and 10% of the degree of cross-linking constant. At the initial stage of polymerization, a thin layer of PMMA shell is deposited on the surface of silica through the copolymerization with the double bonds introduced by MPS. Then, the polymerization of MMA is continuing until MMA is exhausted. Therefore, the thickness of PMMA shells increases with the increased amount of monomer MMA. When the amount of MMA increases from 0.3 g to 0.5 g and to 1.2 g, the thickness of the PMMA shell is increased from 18 nm to 27 nm and to 55 nm (Fig. 5a-c), respectively, and the Fe_3O_4@SiO_2@PMMA microspheres become more and more uniform with more smooth surface. Correspondingly, the thickness of pH-responsive PMAA shell in Fe_3O_4@PMAA microspheres increases obviously with the increasing MMA amount as shown in Fig. 5(d-f). It is observed that the thickness of PMAA shell in Fe_3O_4@PMAA microspheres is slightly thinner than that of PMMA shell in Fe_3O_4@SiO_2@PMMA microspheres, which may be due to the solution of part of linear polymers.

Magnetic and pH-responsive Properties of Corresponding Microspheres

The magnetic property is crucial to magnetic particles for their applications in fast site-specific delivery and separation. Therefore, the magnetic properties of the as-prepared Fe_3O_4 particles, Fe_3O_4@SiO_2, Fe_3O_4@SiO_2@PMMA and Fe_3O_4@PMAA composite microspheres were investigated using a VSM magnetometer at 300 K. As shown in Fig. 6, hysteresis loops show that there is almost no magnetic hysteresis, indicating that Fe_3O_4 particles, Fe_3O_4@SiO_2, Fe_3O_4@SiO_2@PMMA and Fe_3O_4@PMAA composite microspheres reveal superparamagnetic behavior. The saturation magnetization (Ms) values of Fe_3O_4 particles, Fe_3O_4@SiO_2, Fe_3O_4@SiO_2@PMMA and Fe_3O_4@PMAA composite microspheres are 78.2, 44.4, 31.8 and 40.4 emu/g, respectively. The outstanding magnetic property of these corresponding microspheres is most likely due to the supporter core Fe_3O_4 particles consisting of many Fe_3O_4 nanoparticles which resulted in excellent magnetization.[33] The decrease of Ms for composite microspheres may be attributed to the presence of the nonmagnetic silica, PMMA or PMAA shells. However, it should be noted that the Ms of yolk-shell Fe_3O_4@PMAA is larger than that of core-shell-shell Fe_3O_4@SiO_2@PMMA composite microspheres due to the etching of silica interlayer. As illustrated in the inset, the rapid separation of the dispersed Fe_3O_4@PMAA from the aqueous dispersion could be easily visualized within 90 seconds in the presence of an external magnetic field (magnet). Moreover, once the external magnetic field is removed, the Fe_3O_4@PMAA microspheres can be quickly re-dispersed into homogeneous dispersion upon a slight shake. The results show that the higher Ms of the yolk-shell Fe_3O_4@PMAA composite microspheres is particular suitable for targeted drug delivery and other wide applications.

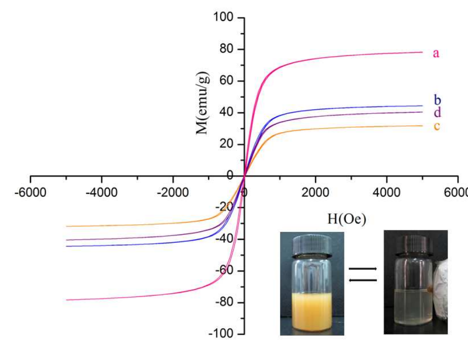

Fig. 6 Magnetic hysteresis loops of (a) Fe_3O_4 particles, (b) Fe_3O_4@SiO_2, (c) Fe_3O_4@SiO_2@PMMA and (d) Fe_3O_4@PMAA composite microspheres. The photograph inset showing the dispersion of yolk-shell Fe_3O_4@PMAA microspheres before (left) and after (right) magnetic separation by an external magnetic field.

For as-prepared yolk-shell Fe_3O_4@PMAA composite microspheres, the PMAA shells with abundant carboxyl groups result in a pH-responsive performance. DLS is used to investigate the pH-responsive behaviour of the yolk-shell structured Fe_3O_4@PMAA microspheres with movable magnetic cores. As shown in Fig. 7, the average hydrodynamic diameter (Dh) of the pH-responsive Fe_3O_4@SiO_2 microspheres increases from 510 nm to 840 nm while the polydispersity index (PDI) of particle size distribution also increases from 0.023 to 0.158 along with the increasing pH values of the dispersion (Table 1). Although PDI increases slightly with the increasing pH values, which may be due to the increasing diameter of swollen PMAA in an alkaline aqueous solution, the considerable small PDI indicates that yolk-shell Fe_3O_4@PMAA microspheres are more uniform in size compared with the previous reports.[40] Moreover, the corresponding zeta potential of Fe_3O_4@PMAA microspheres in a different PBS at pH 4.5, 7.5 and 10 (keeping ionic strength of salt concentration at 0.2 mol L^{-1}) is -2.89, -26.0 and -47.5 mV, respectively. Obviously, the zeta potential becomes more negative with the increasing pH value of the dispersion. These results are owing to the role of –COOH groups in PMAA. When pH<7, the –COOH groups are hardly dissociated, leading to the tightening of curl PMAA chains. With the increase of the pH value, –COOH groups are gradually neutralized into $–COO^-$ anions, leading to the decrease of the zeta potential of Fe_3O_4@PMAA microspheres; at the same time, the polymer chain will become more extended (namely increased swelling degree of the pH-responsive PMAA shell) due to the increased hydrophilicity,[29] resulting in the increased hydrodynamic diameter of yolk-shell Fe_3O_4@PMAA microspheres. The zeta potential and hydrodynamic diameter measurements further reflect that the yolk-shell structured Fe_3O_4@PMAA microspheres are pH dependent.

Table 1 Dh, PDI and zeta potential of the pH-responsive Fe_3O_4@PMAA microspheres in a different PBS at pH 4.5, pH 7.5 and pH 10.

Sample	Dh (nm)	PDI	Zeta potential (mV)
Fe_3O_4@PMAA at pH 4.5	516.7	0.035	-2.89
Fe_3O_4@PMAA at pH 7.5	585.5	0.023	-26.0
Fe_3O_4@PMAA at pH 10	843.8	0.158	-47.5

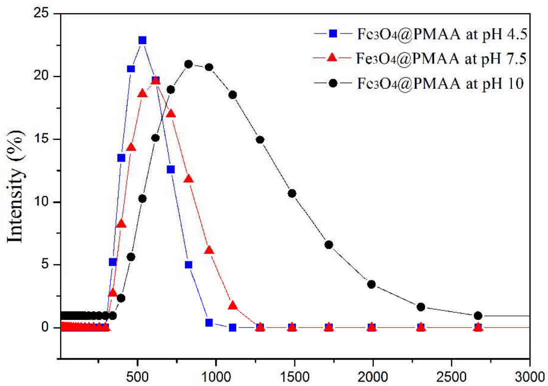

Fig. 7 DLS size distribution profiles of Fe_3O_4@PMAA microspheres in a different phosphate buffer solution at pH=4.5, pH=7.5 and pH=10, respectively.

Metal Ion Adsorption and Regeneration Studies

Fig. 8(a) illustrates the measured adsorption capacities for Cu^{2+}, Pb^{2+}, Cr^{3+} and Cd^{2+} at different pH values by equation (1). To avoid the generation of precipitates such as $Cu(OH)_2$ and $Pb(OH)_2$ at higher pH, the pH values of metal ions solution was limited to less or equal to 7.[41] As shown in Fig. 8, except Cd^{2+}, the yolk-shell Fe_3O_4@PMAA microspheres exhibit a significant adsorption capacity of other metal ions, especially for Cu^{2+} and Pb^{2+}. The adsorption capacity of Cu^{2+} remarkably increased from 0.74 mmol g^{-1} at pH 2 to 3.72 mmol g^{-1} at pH 5, and then decreased to 2.11 mmol g^{-1} at pH 7; while the adsorption capacity of Pb^{2+} remarkably increased from 0.40 mmol g^{-1} at pH 2 to 2.48 mmol g^{-1} at pH 6, and then decreased to 1.82 mmol g^{-1} at pH 7. The variation tendency in the adsorption capacities of Cr^{3+} and Cd^{2+} is similar with those of Cu^{2+} and Pb^{2+}, respectively. The optimum pH value was found to be 5~6. As the pH value of metal ions solution is less than 3, carboxyl groups of PMAA shells are slightly dissociated, so that the weak electrostatic interaction between microspheres and metal ions leads to a low adsorption capacity. With the increase of the pH value, these carboxyl groups are gradually deprotonated and the deprotonation achieves completely at pH value ranging from 5 to 6, resulting in the maximum adsorption capacity. However, at the pH value more than 6, the hydrolysis of the metal ions occurs by the formation of metal hydroxides,[42] which may compete with the uptake of metal ions by the Fe_3O_4@PMAA microspheres, leading to the decrease of adsorption capacity. Thus, the optimum adsorption condition of the Fe_3O_4@PMAA microspheres to Pb^{2+}, Cu^{2+}, and Cd^{2+} is at pH value between 5 and 6. As the concentration of –COOH of the Fe_3O_4@PMAA microspheres is about 3.91 mmol g^{-1} calculated from Fig. S2, which is higher than the adsorption capacity of all metal ions, demonstrating that the adsorption mechanism mainly depend on electrostatic interaction and ion-exchange adsorption.[43] In addition, it is very surprising that the yolk-shell Fe_3O_4@PMAA microspheres exhibit higher capacities than most of other similar adsorbents as compared in Table 2. The reason is owing to the large amount of carboxyl groups in the polymer shells which could absorb metal ions as well as the yolk-shell structures of these Fe_3O_4@PMAA microspheres which also have a profound effect on the adsorption capacities. Therefore, the yolk-shell Fe_3O_4@PMAA microspheres could be widely used as adsorbent in a acid or neutral solutions to absorb Cu^{2+}, Pb^{2+}, Cr^{3+} and Cd^{2+} which are high toxic to organisms and environment, showing a potential application for wastewater treatment.

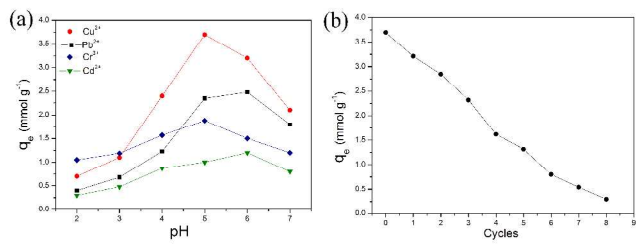

Fig. 8 (a) Effect of pH on the adsorption capacity of Fe_3O_4@PMAA microspheres for different heavy metal ions; (b) Adsorption capacity of Cu^{2+} by Fe_3O_4@PMAA microspheres in the recycling process.

Table 2 Comparison of adsorption capacity (mmol g^{-1}) for heavy metal ions on yolk-shell Fe_3O_4@PMAA microspheres with other similar adsorbents.

Similar Adsorbents	Adsorption capacities (mmol g^{-1})	Number of cycles	Reference
Fe_3O_4@PMAA yolk-shell microspheres	Pb^{2+}: 2.48 Cu^{2+}: 3.72 Cd^{2+}: 1.24 Cr^{3+}: 1.68	8	This work
Poly(ethylenediamine) dots@SiO_2	Cu^{2+}: 3.87	--	32
Amino-functionalized Fe_3O_4@SiO_2 core-shell microspheres	Pb^{2+}: 0.54 Cu^{2+}: 0.69 Cd^{2+}: 0.33	4	44
PAA/GO/Fe_3O_4 nanocomposites	Pb^{2+}: 1.45 Cu^{2+}: 2.08 Cd^{2+}: 1.17	5	31
EDTA-Functionalized Silica Spheres	Cu^{2+}: 0.47 (26 mg g^{-1}) Cd^{2+}: 0.13 (15 mg g^{-1})	3	45
Fe_3O_4@SiO_2@meso-SiO_2-NH_2 microsphere	Pb^{2+}: 1.40 (289.7 mg g^{-1}) Cu^{2+}: 3.01 (196.5 mg g^{-1}) Cd^{2+}: 1.37 (154.2 mg g^{-1})	5	46
chitosan/poly(acrylic acid) magnetic microspheres	Cu^{2+}: 2.71 (174 mg g^{-1})	6	47

As shown in Fig. 8(b), the adsorption capacity is reduced by 11% in the first desorption-adsorption cycle compared with the original adsorption capacity, while the decrease of adsorption capacity was not more than 15% in the next 7 cycles. However, by the analyses of atomic emission spectra, the desorption rate of Cu^{2+} from Cu^{2+}-Fe_3O_4@PMAA microspheres is about 88%-92% compared with the last adsorption cycle, which indicates that the adsorption capacity of Fe_3O_4@PMAA microspheres for the metal ions is hardly reduced. The decrease of adsorption capacity in recycling is actually due to residual metal ions in microspheres after desorption and the inevitable loss of adsorbent in experimental operation. Therefore, our magnetic and pH-responsive adsorbents can be readily recycled from the waste water and then reused for several times with high adsorption capacity, promising its great potential in practical application.

The influence of the thickness of PMAA shells and void space of yolk-shell Fe_3O_4@PMAA microspheres on the adsorption of metal ions is studied to gain further insight into the adsorption process. As shown in Table S1, when the thickness of PMAA shells increases from 15 to 25 then to 40 nm, the adsorption capacity of Pb^{2+} at pH 6 is promoted from 1.02 to 1.87 then to 2.48 mmol g^{-1}. This reason can be attributed to the increased –COOH groups along with the increase of the thickness of PMAA shells. As the void space of Fe_3O_4@PMAA increases from 0.024 to 0.058 μm^3, the adsorption capacity of Pb^{2+} at pH 6 is promoted from 1.98 to 2.45 mmol g^{-1}. However, when the void space further increases to 0.13 μm^3, the adsorption capacity of Pb^{2+} is only promoted a little (2.48 mmol g^{-1}). It indicates that only enough void space is beneficial to the adsorption of metal ions though electrostatic interaction with $–COO^-$ groups in the inner wall of PMAA shells. Therefore, the optimum yolk-shell Fe_3O_4@PMAA microspheres for the adsorption of metal ions in our experimental conditions are those with the thickness of PMAA shells about 40 nm and void space of not less than 0.058 μm^3.

Drug Loading and Controlled Release

To evaluate the feasibility of Fe_3O_4@PMAA yolk-shell microspheres as drug delivery carriers, ceftriaxone sodium (CTX), a water soluble anti-inflammatory drug, was chosen as a model drug for loading and controlled release. CTX in salt form might interact with the Fe_3O_4@PMAA microspheres by the electrostatic interaction between the protonated amine cation of the drugs and the carboxylate anion of the carries, meanwhile, hydrophilic interactions between the carries and the drugs was also existed. UV-Vis absorption spectroscopy was used to determine the effective CTX load capacity and releasing behavior. Fig. 9(a) shows the absorption spectra of a CTX aqueous solution[48] before and after adding Fe_3O_4@PMAA microspheres. It can be seen that the absorption peak at 235 nm of CTX disappears, and the absorbance of the characteristic peak at 272 nm greatly decreases after adding Fe_3O_4@PMAA microspheres. It indicates that the CTX molecules have been loaded into the Fe_3O_4@PMAA microspheres, resulting in a significant decrease of the drug concentration in solution. We calculated the drug loading capacity (DLC) of the Fe_3O_4@PMAA microspheres with about 180% by equation (2) according to the standard curve of CTX solution as shown in Fig. S3, which is attributed to the carboxylic acid groups of PMAA shells and the void space of the microspheres. It is worth noting that the DLC of the yolk-shell Fe_3O_4@PMAA microspheres is higher than that obtained in the previous reports.[49] Because the electrostatic interactions between the negatively charged PMAA shells and positively charged CTX are so strong, the positively charged CTX will permeate through the negatively charged PMAA shells into void space of the microspheres when CTX is added into the dispersion of Fe_3O_4@PMAA microspheres. Due to the pH-responsive property of PMAA shells, the CTX drug release at a different pH phosphate buffer solution (pH=4.5 and pH=7.5) is shown in Fig. 9 (b). The drug release curves reveal that the release rate is pH- dependent and increases with the decrease of pH values. The cumulative release amount of CTX could reach up to 74% after 48 h in a PBS at pH 4.5, which is much higher than that at pH 7.5 (only 33%). This is because once the pH value of the medium decreases, the carboxylate anion of the negatively charged PMAA shells would be protonated to form uncharged free carboxylic acid and thus the electrostatic interaction would disappear.

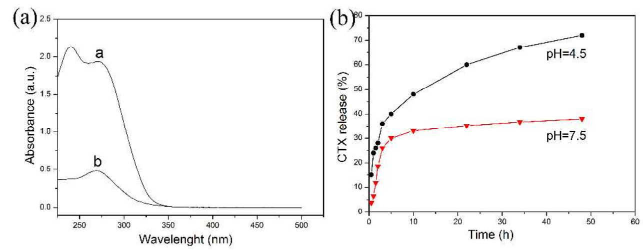

Fig. 9 (a) UV-Vis absorption spectra of solutions before a) and after b) adding Fe_3O_4@PMAA yolk-shell microspheres; (b) CTX-release curves for CTX-loaded Fe_3O_4@PMAA yolk-shell microspheres in a different PBS at pH 4.5 and pH 7.5 at 37°C, respectively.

The effect of the thickness of PMAA shells and void space of Fe_3O_4@PMAA microspheres on DLC and controlled release is also investigated. As shown in Table S1, the effect of thickness of PMAA shells and void space of Fe_3O_4@PMAA microspheres on DLC is similar with that on the adsorption of metal ions, which demonstrates that the optimum yolk-shell Fe_3O_4@PMAA microspheres for DLC are the same as above. However, Fig. S4 shows that the thickness of PMAA shells and void space of Fe_3O_4@PMAA microspheres have no significant effect on the CTX-release behavior at pH 4.5 with the cumulative release amount of CTX only ranging from 83% to 72%. The reason may be that the drug delivery process mainly depends on the relieving of the electrostatic interaction between PMAA and CTX. Furthermore, the thinner the PMAA shell is, the higher is the cumulative release amount of CTX at pH 4.5, which may be attributed to that the carboxylic groups in the thin PMAA shells are easily protonized adequately at a relative weak acidity, leading to the weakening of electrostatic attraction between PMAA and CTX.

Conclusions

In summary, bi-functional and monodisperse yolk-shell structured Fe_3O_4@PMAA composite microspheres with both high magnetization and pH-responsive property have been successfully synthesized in high yield through a simple "silica-assisted" etching strategy. The shell thickness and void space of yolk-shell magnetic Fe_3O_4@PMAA microspheres can be tuned by controlling the amounts of MMA and TEOS, respectively. The yolk-shell Fe_3O_4@PMAA microspheres can be used as adsorbent for metal ions and drug carriers, which demonstrate the high adsorption capacity and reusability for heavy metal ions, drug loading capacity and good controlled drug release. In addition, the adsorption capacities and drug delivery could be tailored by changing the thickness of PMAA and void space of yolk-shell Fe_3O_4@PMAA microspheres. This facile synthesis strategy can be easily extended to the synthesis of other encapsulated materials (e.g. Fe_2O_3, carbon nanotubes, Ag and so on) with the stimuli-responsive polymers and the unique yolk-shell structure.

Acknowledgements

This work is supported by the National Natural Science Foundation of China (Project No. 21074122, 51373160 and 50873096).

Notes and references

Department of Polymer Science and Engineering, CAS Key Laboratory of Soft Matter Chemistry, University of Science and Technology of China, Hefei, Anhui 230026, China. E-mail: hrliu@ustc.edu.cn; Tel: +86 551 63601586

†Electronic supplementary information (ESI) is available including the FTIR analysis of Fe_3O_4@PMAA microspheres in a different phosphate buffer solution, conductivity titration curve of yolk-shell Fe_3O_4@PMAA microspheres, the calibration curve of Ceftriaxone sodium solution, and the influences of the thickness of PMAA shells and void space of Fe_3O_4@PMAA microspheres on adsorption of metal ions and drug delivery.

1. Z. Chen, Z. Li, Y. Lin, M. Yin, J. Ren and X. Qu, *Chem. Eur. J.*, 2013, **19**, 1778.
2. L. Gao, J. Fei, J. Zhao, W. Cui, Y. Cui and J. Li, *Chem. Eur. J.*, 2012, **18**, 3185.
3. B. Liu, W. Zhang, H. Feng and X. Yang, *Chem. Commun.*, 2011, **47**, 11727.
4. H. Pang, P. Cheng, H. Yang, J. Lu, C. X. Guo, G. Ning and C. M. Li, *Chem. Commun.*, 2013, **49**, 1536.
5. N. Liu, H. Wu, M. T. McDowell, Y. Yao, C. Wang and Y. Cui, *Nano Lett.*, 2012, **12**, 3315.
6. J. Liu, S. Z. Qiao, J. S. Chen, X. W. Lou, X. Xing and G. Q. Lu, *Chem. Commun.*, 2011, **47**, 12578.
7. J. Lee, J. C. Park and H. Song, *Adv. Mater.*, 2008, **20**, 1523.
8. D. P. Wang and H. C. Zeng, *Chem. Mater.*, 2009, **21**, 4811.
9. S. Xing, L. H. Tan, T. Chen, Y. Yang and H. Chen, *Chem. Commun.*, 2009, 1653.
10. X. J. Wu and D. Xu, *J. Am. Chem. Soc.*, 2009, **131**, 2774.
11. Q. Fang, S. Xuan, W. Jiang and X. Gong, *Adv. Funct. Mater.*, 2011, **21**, 1902.
12. Y. Yang, J. Liu, X. Li, X. Liu and Q. Yang, *Chem. Mater.*, 2011, **23**, 3676.
13. B. Luo, X.-J. Song, F. Zhang, A. Xia, W. L. Yang, J. H. Hu and C. C. Wang, *Langmuir*, 2009, **26**, 1674.
14. J. Liu, J. Cheng, R. Che, J. Xu, M. Liu and Z. Liu, *ACS Appl. Mater. Interfaces*, 2013, **5**, 2503.
15. S. Wu, J. Dzubiella, J. Kaiser, M. Drechsler, X. Guo, M. Ballauff and Y. Lu, *Angew. Chem. Int. Ed.*, 2012, **51**, 2229.
16. B. Liu, W. Zhang, F. Yang, H. Feng and X. Yang, *J. Phys. Chem. C*, 2011, **115**, 15875.
17. G. Liu, J. Gao, H. Ai and X. Chen, *Small*, 2013, **9**, 1533.
18. D. N. Nguyen, J. J. Green, J. M. Chan, R. Longer and D. G. Anderson, *Adv. Mater.*, 2009, **21**, 847.
19. C. D. H. Alarcon, S. Pennadam and C. Alexander, *Chem. Soc. Rev.*, 2005, **34**, 276.
20. L. Guo Liang, T. Chin An, K. G. Neon, E. T. Kang and Y. Xinlin, *Polym. Chem.*, 2011, **2**, 1368.
21. K. Paek, S. Chung, C. H. Cho and B. J. Kim, *Chem. Commun.*, 2011, **47**, 10272.
22. L. Zhang, T. Wang, L. Li, C. Wang, Z. Su and J. Li, *Chem. Commun.*, 2012, **48**, 8706.
23. T. Yao, T. Cui, X. Fang, J. Yu, F. Cui and J. Wu, *Chem. Eng. J.*, 2013, **225**, 230.
24. F. Bai, B. Huang, X. Yang and W. Huang, *Eur. Polym. J.*, 2007, **43**, 3923.
25. Y. Li, M. Dong, J. Kong, Z. Chai and G. Fu, *J. Colloid. Interface Sci.*, 2013, **394**, 199.
26. G. L. Li, C. A. Tai, K. G. Neoh, E. T. Kang and X. Yang, *Polym. Chem.*, 2011, **2**, 1368.
27. E. Bourgeat-Lami and M. Lansalot, Adv. Polym. Sci, 2010, **233**, 53.
28. A. M. Santos, J. Guillot and T. F. McKenna, *Chem. Eng. Sci.*, 1998, **53**, 2143.
29. J. F. Tan, A. Blencowe, T. K. Goh, I. T. M. Dela Cruz and G. G. Qiao, *Macromolecules*, 2009, **42**, 4622.
30. K. Kadirvelu, C. Faur-Brasquet and P. Le Cloirec, *Langmuir*, 2000, **16**, 8404-8409.
31. W. Zhang, X. Shi, Y. Zhang, W. Gu, B. Li and Y. Xian, *Journal of Materials Chemistry A*, 2013, **1**, 1745-1753.
32. Z.-A. Qiao, Q. Huo, M. Chi, G. M. Veith, A. J. Binder and S. Dai, *Adv. Mater.*, 2012, **24**, 6017.
33. S. Xuan, Y. X. J. Wang, J. C. Yu and K. C. F. Leung, *Chem. Mater.*, 2009, **21**, 5079.
34. Y. Deng, D. Qi, C. Deng, X. Zhang and D. Zhao, *J. Am. Chem. Soc.*, 2008, **130**, 28.
35. X.-G. Li, H. Feng and M.-R. Huang, *Chem. Eur. J.*, 2009, **15**, 4573.
36. J. Ge, Y. Hu, M. Biasini, W. P. Beyermann and Y. Yin, *Angew. Chem. Int. Ed.*, 2007, **46**, 4342.
37. S. Libert, V. Gorshkov, D. Goia, E. Matijevkic and V. Privman, *Langmuir*, 2003, **19**, 10679.
38. W. Yi, G. Bao-Hua, W. Xian, X. Jun, W. Xin and Z. Yin-Ping, *Polymer*, 2009, **50**, 3361.
39. T. Kida, M. Mouri and M. Akashi, *Angew. Chem. Int. Ed.*, 2006, **45**, 7534.
40. W. H. Chiang, H. Viet Thang, H. H. Chen, W. C. Huang, Y. F. Huang, S. C. Lin, C. S. Chern and H. C. Chiu, *Langmuir*, 2013, **29**, 6434.
41. W. N. Perera, G. Hefter and P. M. Sipos, *Inorg. Chem.*, 2001, **40**, 3974.
42. S. Veli and B. Alyuez, *J. Hazard. Mater.*, 2007, **149**, 226.
43. L. X. Zhong, X. W. Peng, D. Yang and R. C. Sun, *J. Agric. Food Chem.*, 2012, **60**, 5621.
44. J. Wang, S. Zheng, Y. Shao, J. Liu, Z. Xu and D. Zhu, *J. Colloid. Interface Sci.*, 2010, **349**, 293.
45. D. Q. Melo, V. O. S. Neto, J. T. Oliveira, A. L. Barros, E. C. C. Gomes, G. S. C. Raulino, E. Longuinotti and R. F. Nascimento, *J. Chem. Eng. Data*, 2013, **58**, 798.
46. Q. Yuan, Y. Chi, N. Yu, Y. Zhao, W. Yan, X. Li and B. Dong, *Mater. Res. Bull.*, 2014, **49**, 279.
47. H. Yan, L. Yang, Z. Yang, H. Yang, A. Li and R. Cheng, *J.Hazard. Mater.*, 2012, **229**, 371.
48. D. G. Sankar, N. Sujatha, B. A. Kumar and P. V. Madhavilatha, *Asian J. Chem.*, 2006, **18**, 3244.
49. L. Li, L. Zhang, S. Xing, T. Wang, S. Luo, X. Zhang, C. Liu, Z. Su and C. Wang, *Small*, 2013, **9**, 825.